2,2′-Bipyridyl-3,3′-diol Incorporated into $AlPO_4$-5 Crystals and Its Spectroscopic Properties as Related to Aqueous Liquid Media

Knut Rurack,*,† Katrin Hoffmann,† Wajih Al-Soufi,‡ and Ute Resch-Genger†

Department I.3902, Bundesanstalt für Materialforschung und -prüfung (BAM), Richard-Willstätter-Strasse 11, D-12489 Berlin, Germany, and Departamento de Química Física, Facultade de Ciencias, Universidade de Santiago de Compostela, Campus Universitario s/n, E-27002 Lugo, Spain.

Received: April 17, 2002; In Final Form: June 26, 2002

A novel fluorescent host−guest material, molecular sieves of $AlPO_4$-5-type doped with 2,2′-bipyridyl-3,3′-diol, was prepared and spectroscopically characterized. The composite crystals show a pronounced optical anisotropy, indicating a high degree of alignment of the guest molecules within the zeolitic pore system. A mean tilting angle of 22° was found for the orientation of the individual dye molecules in the straight channels. The corrected fluorescence emission spectra were determined, and time-resolved fluorescence studies revealed that the dye molecules are preferentially found in three different types of microenvironment. By invoking pH-dependent studies of the dye in aqueous solution, we could trace these spectroscopic features back to two main influences, coadsorbed water within $AlPO_4$-5 pores and guest−host interactions with a few relatively weak Brønsted acid (defect) sites of the inorganic host network.

Introduction

The incorporation of organic dye molecules into organic,[1] inorganic,[2] or hybrid[3] hosts is of particular interest in many different areas of materials and analytical chemistry. Potential fields of application include the development of photonic devices and materials such as laser[4] and recording[5] media, optical switches,[6] artificial antenna systems,[7] or electrochromic devices,[8] as well as the construction of optical sensors.[9] Among host−guest assemblies, zeolites and zeolitic molecular sieves are solid hosts with unique properties. Because molecular sieves are optically transparent in a wide spectral range, the excitation of organic guest molecules is possible without affecting the electronic structure of the host material. The perfect geometric pore system of the crystalline matrix also provides specific intrazeolitic adsorbate systems. The confined space within zeolite channels supports highly dispersed arrangements of guest molecules, preventing the formation of dimers or dye aggregates.[10,11] One of the main advantages of introducing organic dye molecules to solid host materials is improved dye stability. Incorporated guests are to a certain degree protected against photobleaching, thermal decomposition, and attack by reactive species from the environment, resulting in enhanced photophysical and photochemical stability.[12]

Besides materials chemistry-based aspects, for applicational use and design, a better understanding of network−guest interactions is very helpful. In the case of porous materials for potential optical applications, the introduction of fluorescent dye molecules that are sensitive to certain microenvironmental parameters promises to obtain more information on internal host properties. So far, various fluorescent probes have been used, mostly in cavity-type zeolites, to reveal details of the structure of host/guest materials.[13] Reporter molecules that show an excited-state intramolecular proton transfer (ESIPT) and subsequent fluorescence of the proton-transfer species should be especially suited to monitor microenvironmental features such as polarity, surface acidity, or water accessibility of the host system, because their spectroscopic properties are strongly influenced by any kind of proton activity of the host's medium.

In the present work, we chose 2,2′-bipyridyl-3,3′-diol ($BP(OH)_2$) as the fluorescent dopant within an $AlPO_4$-5 molecular sieve.[14] On one hand, $BP(OH)_2$ is a suitable fluorescent guest because it is a comparatively stable organic dye molecule and was proposed for use as both a laser dye[15] and a fluorescence standard.[16] On the other hand, favorable spectroscopic features such as strongly Stokes-shifted, broad, and structureless absorption and emission bands, as well as a high fluorescence yield of this ESIPT dye (Scheme 1) in aprotic solvents, are strongly influenced in the presence of hydrogen bond donating solvents.[17,18] Thus, the spectroscopic behavior of encapsulated $BP(OH)_2$ should allow us to probe the microenvironment of the molecular sieve $AlPO_4$-5. Here, we report on the preparation of $BP(OH)_2$-doped $AlPO_4$-5 crystals and their optical spectroscopic properties as investigated at the single-crystal and the crystal-ensemble level, relating the results to the dye's behavior in various solvents of different proticity and acidity.

Experimental Section

Materials. $BP(OH)_2$, purchased from Aldrich, was recrystallized from light petroleum and checked for purity by HPLC. Dichloromethane (Aldrich) was of UV-spectroscopic grade; analysis-grade HCl (37 wt %) and NaOH were both obtained from Merck and bidistilled water was provided by the Laboratory for Trace Elemental Analysis, BAM, Berlin. The solvents used in the molecular sieve loading process, 1,3,5-triisopropylbenzene and acetone, were purchased from Aldrich. Large and optically transparent $AlPO_4$-5 molecular sieve crystals of perfect hexagonal shape (ca. 10 μm × 50 μm)[19] were used as host material. The composites were prepared after calcination of the as-synthesized host material $AlPO_4$-5 at 600 °C for at least 9 h

* To whom correspondence should be addressed. E-mail: knut.rurack@bam.de. Fax: 49-(0)30-8104 5005.
† Bundesanstalt für Materialforschung und -prüfung.
‡ Universidade de Santiago de Compostela.

10.1021/jp0259622 CCC: $22.00
Published on Web 08/28/2002

SCHEME 1. Simplified Schematic Description of the Main Proton Transfer Features of $BP(OH)_2$ upon Absorption of a Photon[a]

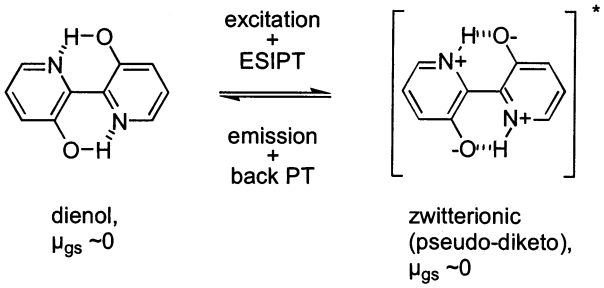

[a] An ultrafast excited-state intramolecular (double) proton transfer (ESIPT) occurs. Radiative deactivation of the zwitterionic ESIPT form is then followed by a back PT, yielding the initial ground-state dienol tautomer.

in normal (air) atmosphere. This calcination process is necessary to remove structure-directing organic template molecules from the molecular sieve channels that have been incorporated during synthesis. After cooling to 50 °C, $BP(OH)_2$ was introduced into the molecular sieve pores by adding the host material to a solution of 0.3% $BP(OH)_2$ in 1,3,5-triisopropylbenzene. The resulting suspension was stirred for 5 h at 110 °C. The slightly yellow molecular sieve crystals were filtered, washed with acetone, and then dried at room temperature.

Absorption and Fluorescence Microspectroscopy of the Doped Crystals. The absorption and fluorescence spectra of selected $AlPO_4$-5 crystals were recorded with a microscope spectral photometer UMSP 80 (Carl Zeiss, Oberkochen, Germany) with quartz optics. The measurements were performed in the region of 300−800 nm using a 75 W xenon lamp dispersed by a grating monochromator (spectral bandwidth 5 nm). The illuminated area was reduced to the approximate crystal size by a diaphragm and the minimum diameter of the measurement spot was limited by a Zeiss objective Ultrafluar 10/2 (10×) to 5 μm. For polarization-dependent UV/vis spectra, the transmitted light was analyzed by a Glan polarizer in the microscope tube. The alignment of the polarizer with respect to the hexagonal long axis of $AlPO_4$-5 molecular sieve crystals was determined with an accuracy of <1°.

Fluorescence measurements were performed with an epifluorescence attachment. The Zeiss filter set employed included a 365 nm excitation band-pass filter, the dichroic beam splitter FT 395 nm, and the barrier filter LP 420 nm, the latter enabling emission measurements above 420 nm.

Laser Impulse Fluorometry of the Doped Crystals. The laser-excited fluorescence emission spectra were recorded with a unique laser impulse fluorometer with time-correlated single-photon counting detection described elsewhere.[20] The sample was excited with the second harmonic output (LBO crystal) of a regenerative mode-locked argon ion laser-pumped Ti:sapphire laser at a repetition rate of 4 MHz (reduction by synchronized pulse selection). The samples prepared for the microscopy experiments were mounted on an *X*,*Y*,*Z*-stage (micromanipulator 3301R from World Precision Instruments) parallel to the plane of the entrance slit of the emission monochromator (Figure S1A, Supporting Information). To minimize scattered excitation light and background fluorescence, a mask with a small aperture (2 mm) was fixed at the side of the sample facing the detection unit (Figure S1A,B). For each sample, the laser beam was directed through the mounted ensemble from the rear and the front at angles of approximately 45° (Figure S1A). The emission was monitored with a subtractive double monochromator (spectral bandwidth of 8 nm). The excitation energies were adjusted with a double prism attenuator from LTB and checked with a calibrated Si diode (model 221 with 100:1 attenuator 2550, Graseby) and an optometer (model S370, Graseby). In a typical experiment, the pulse peak power was 5×10^{-2} W, that is, with excitation at 390 nm the sample was excited with ca. 10^5 photons per pulse.

The fluorescence spectra were recorded in the range of 400−700 nm with increments of 1 nm, and photons were counted for 1 s at each step. Calibration of the spectral response of the detection system was performed with a calibrated quartz halogen lamp placed inside an integrating sphere (Gigahertz-Optik). The calibration was checked by a comparison of the fluorescence spectra of quinine sulfate dihydrate (NIST standard reference material SRM 936) in 0.105 M $HClO_4$ recorded on the laser impulse fluorometer and on a calibrated steady-state Spectronics Instruments 8100 spectrofluorometer.

The fluorescence decays were recorded at various wavelengths within the fluorescence band with a time division of 5.2 ps channel^{-1}. The instrumental response function of the system was typically 30 ps (full width at half-maximum), and the decay times were obtained with an experimental accuracy of ±3 ps. The temporal calibration of the experimental setup is described in detail in ref 21. The fluorescence lifetime profiles were analyzed with a PC using the software packages FLA 900/Level 2 (Edinburgh Instruments; for lifetime distribution analysis of single decays) and Global Unlimited V2.2 (Laboratory for Fluorescence Dynamics, University of Illinois; for global decay profile analysis). The goodness of the fit of the single decays was judged by reduced chi-squared (χ_R^2) and the autocorrelation function $C(j)$ of the residuals. Within the global analysis of the decays recorded at different emission wavelengths, the decay times of the species are linked, while the program varies the preexponential factors and lifetimes until the changes in the error surface (χ^2 surface) are minimal, that is, convergence is reached. The fitting results are judged for every single decay (local χ_R^2) and for all of the decays (global χ_R^2). Except as otherwise indicated, the errors for all of the measurements presented here were below global $\chi_R^2 = 1.2$.

UV/vis Spectrophotometry and Fluorometry in Solution. UV/vis spectra were recorded on a Carl Zeiss Specord M400/M500 absorption spectrometer, and steady-state emission spectra were obtained with a Perkin-Elmer LS50B spectrofluorometer. All of the measurements were performed with dilute solutions (optical density ≤ 0.05), and the fluorescence spectra reported here are corrected for the spectral responsivity of the emission channel. The detailed calibration procedure of the fluorometer is described in ref 21. The time-resolved fluorescence solution data were measured at the Berlin Storage Ring for Synchrotron Radiation (BESSY). The pulsed excitation source BESSY allowed for a temporal resolution of ca. 100 ps (single-bunch mode, 4.8 MHz), and the excitation wavelength of the synchrotron radiation was selected with a monochromator with 4 nm spectral bandwidth. The emission monochromator was usually set at a spectral bandwidth of 8 nm. The fluorescence decay curves were recorded in a time-correlated single-photon timing mode with a time division of 55.5 ps channel^{-1} and an experimental accuracy of ±0.04 ns. The instrumental setup is described in detail in ref 22.

pH Measurements and pK_a Determination. The spectrophotometric pH titration was carried out in 50 mm quartz cells by addition of small amounts of various undiluted and diluted HCl solutions, prepared from 10 M (37 wt %) HCl, with microliter pipets (Eppendorf). After stirring for 2 min, the pH

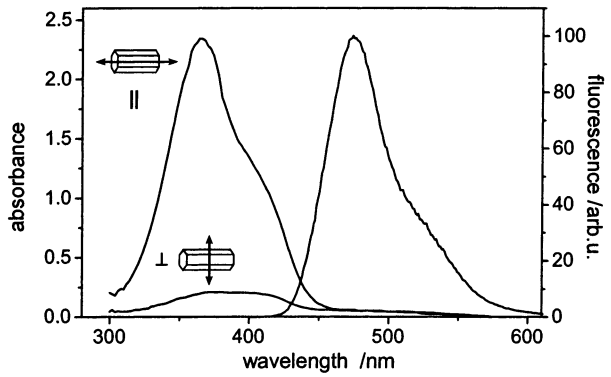

Figure 1. Steady-state emission spectrum (uncorrected) of an individual $BP(OH)_2$-containing $AlPO_4$-5 crystal excited at 365 nm and anisotropic absorbance of $BP(OH)_2$ within the one-dimensional pore system. The polarization of light parallel or perpendicular to the hexagonal *z*-axis of the $AlPO_4$-5 crystals is indicated by arrows.

was monitored employing a digital pH meter (WTW pH 537) equipped with a glass electrode (Mettler Toledo InLab 423). Calibration of the instrument was performed with standard aqueous solutions of pH = 1.68, 4.01, 6.86, and 9.18 from WTW. For these experiments, the absorption spectrum was recorded every 0.25 pH units. The pK_a values were first estimated roughly from the absorption titration data by a graphical method described in more detail in section A of the Supporting Information. Then, precise pK_a values were determined by applying principal component global analysis (PCGA).[23] PCGA allows in a first step to reliably determine the number of absorbing species with different pure spectra (components). In a second step, the parameters of a reaction model are adjusted globally to all of the experimental data, taking into account the previously determined components. This leads to a thorough analysis of the data with precise pK_a values and species spectra. A self-developed program was used for PCGA.

Results

Microscope Spectroscopy of the Doped Crystals. The electronic spectra of molecular sieve-encapsulated $BP(OH)_2$ obtained by microscope spectroscopy of several individual $AlPO_4$-5 crystals are shown in Figure 1.[24] The main absorption and emission bands at 365 and 474 nm lie in the same region as those for the dye in isotropic media, and the features of broad and structureless bands are also preserved in the crystal (Figure 1, cf. Figure 5 below, Table 1). However, polarization-dependent measurements reveal the constraints imposed by the rigid host upon the guest molecules. The composite crystals show a pronounced optical anisotropy when the absorption is monitored parallel and perpendicular to the straight channels of $AlPO_4$-5, resulting in a small dichroic ratio $d = A_\perp(\tilde{\nu})/A_\parallel(\tilde{\nu})$ of 0.08.

In the spectral range considered, $BP(OH)_2$ has only one relevant transition moment polarized parallel to the molecular long axis,[25] and thus, the tilt angle θ of the adsorbate molecules with respect to the one-dimensional pore structure[14] of the molecular sieve can be calculated from the dichroic ratio according to $\tan^2\theta = 2d$.[26] On the basis of the measurements presented in Figure 1, a mean tilt angle $\langle\theta\rangle = 22°$ is obtained for the orientation of the individual $BP(OH)_2$ molecules in the straight $AlPO_4$-5 channels. The strong polarization-dependent absorption indicates a high degree of alignment of the guest molecules within these channels, the slightly tilted molecular long axis of $BP(OH)_2$ being virtually parallel to the straight pore system of the host crystals.

Laser-Excited Fluorescence Properties of the Doped Crystals. The corrected fluorescence emission spectra of an ensemble of $BP(OH)_2$-doped $AlPO_4$-5 crystals, excited at 393 and 419 nm, respectively, with the laser impulse fluorometer, are shown in Figure 2. The spectrum excited at 419 nm (circles) could be fitted (dashed line) employing a single log-normal function, and for the fluorescence spectrum obtained upon 393 nm excitation, only at the far blue edge at ca. 425 nm, a very weak shoulder is observed. The shapes of both spectra are virtually identical and suggest that the major emitting species formed are largely similar for both excitation wavelengths. Moreover, no differences were found for rear or front face excitation of the ensembles (see Experimental Section for details), and excitation intensity-dependent experiments in the nanowatt to microwatt range (average laser power)[27] revealed no changes in the fluorescence spectra and lifetimes, indicating the absence of pronounced photobleaching.

The fluorescence decays recorded at various emission wavelengths between 435 and 555 nm (for 393 nm excitation) or 455 and 575 nm (excitation at 419 nm) are always nonexponential (Figure S3). When analyzing the data by single-decay fitting procedures employing discrete lifetimes,[28] in all of the cases, three exponents were necessary to obtain acceptable fits. Global analyses[28,29] also yielded acceptable results only when three discrete decay-associated species were introduced. Furthermore, none of the analyses indicated the presence of a photochemical reaction[30] between these species during their excited-state lifetime on the >10 ps scale detectable with our instrumental setup.

The species diversity encountered when trying to fit the time-resolved emission data with the aid of discrete decay times suggests that the individual dye molecules are strongly influenced by their immediate microscopic environment. In such a case, another model, which is based on the assumption that in the ensemble the molecular emitter shows a quasi-continuous distribution of lifetimes or reaction rates, can be utilized to recover the decay kinetics.[31] This procedure can thus yield more reliable results when the microenvironmental properties such as, for instance, pore size or (inner) surface structure are rather heterogeneous and not evenly distributed yet strongly dominate the excited-state behavior of the fluorophore. The envelope of such a lifetime distribution function usually shows several peaks, corresponding to the average lifetimes, $\langle\tau\rangle$, (or centers of gravity) of certain preferred species or environmental situations, and each of the peaks is characterized by a specific width σ.[32] In the past few years, this strategy was successfully applied to describe the dynamic fluorescence behavior of cyclodextrin inclusion complexes,[33] micelle systems,[32] and surface-bound fluorophores[34] or the behavior of dyes in polymers or aggregates.[35]

Figure 3 represents a typical distribution function as obtained for a $BP(OH)_2$-doped $AlPO_4$-5 ensemble with parameters $\langle\tau_1\rangle = 0.23$ ns ($\sigma = 0.09$ ns), $\langle\tau_2\rangle = 0.88$ ns ($\sigma = 0.30$ ns), and $\langle\tau_3\rangle = 3.65$ ns ($\sigma = 0.94$ ns) for the three peaks. However, the relative contributions of the three peaks to the overall intensity as a function of the observation wavelength show a more specific trend (Figure 4). Whereas the fast decaying species gain in intensity with increasing emission wavelength, no such trend is observed for the intermediate components centered around $\langle\tau_2\rangle \approx 0.85$ ns. Accordingly, the slow decay component contributes less at longer emission wavelengths.[36]

The absorption, as well as steady-state and time-resolved fluorescence, data suggest that incorporation of fluorescent dyes capable of intramolecular proton transfer into zeolites can gain more information on the inner surface structure of potentially

TABLE 1: Spectroscopic Data of $BP(OH)_2$ in Various Media (Shoulders in the Spectra Are Given in Parentheses)

	medium	$\tilde{\nu}_{abs}$ (10^3 cm^{-1})	$\tilde{\nu}_{em}$ (10^3 cm^{-1})	$\Delta\tilde{\nu}_{abs-em}$ (cm^{-1})	τ_f (ns)
$BP(OH)_2$	$AlPO_4-5$	27.4,[a] (24.6)	21.1[b]	6300	see text
	n-hexane[c]	29.2	19.8	9400	3.1
	CH_2Cl_2[d]	29.4	19.9	9500	3.2
	ethanol[c]	29.4	20.7	8700	2.1
	H_2O, pH 6.4	28.8,[e] 24.8 (23.2)	21.3 (23.6)	7500	0.45, 4.8[f]
	H_2O, pH 2.0	27.5,[g] (24.8)	21.0	6500	0.7
	H_2O, pH 11.5	32.0	(23.5, 20.2)[h]	10 000	0.08[i]
Zn^{II} complex	H_2O[j]	27.5	22.5	5000	6.17

[a] Global maximum, ratio of 27.4:24.6 = 1.3:1. [b] Uncorrected. [c] From ref 18c; fluorescence quantum yields $\Phi_f = 0.30$ in hexane and 0.18 in EtOH. [d] $\Phi_f = 0.21$ in CH_2Cl_2. [e] Global maximum (see Figure 5), ratio of 28.8:24.8:23.2 = 2.4:1.4:1. [f] Relative amplitudes vary with excitation and emission wavelength and are always >0.98 for the fast component. [g] Global maximum, ratio of 27.5:24.8 = 5.2:1. [h] Weak and very broad band, most probably composed of various subbands, with a shape that is strongly dependent on excitation wavelength. [i] Major component with a relative amplitude >0.8 at all combinations of excitation (333 and 377 nm) and emission (440, 465, and 518 nm) wavelengths employed at pH = 10.3; at higher pH with further decreased fluorescence quantum yields (<0.01), the temporal resolution of the excitation source BESSY was the limiting factor for a reliable determination of the fast fluorescence lifetimes (see Experimental Section). [j] From ref 18c; $\Phi_f = 0.62$.

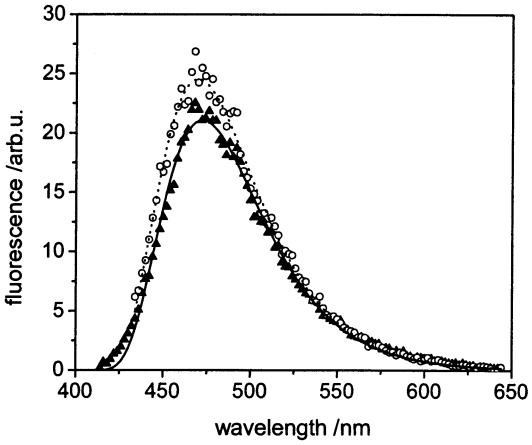

Figure 2. Corrected fluorescence spectra of a powder sample of $BP(OH)_2$ encapsulated in $AlPO_4$-5 and excited at 393 (▲) and 419 nm (○). The log-normal fits of the main bands are included (solid and dotted lines).

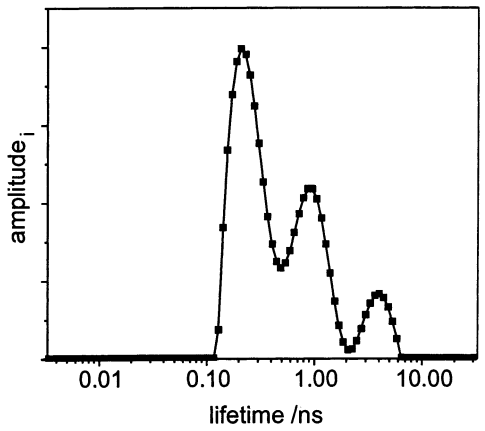

Figure 3. Lifetime distribution of $BP(OH)_2$ in $AlPO_4$-5 excited and recorded at 393 and 515 nm.

hydrogen-acidic inorganic hosts. The situation within this particular aluminum phosphate molecular sieve host with respect to hydrogen acidity can be rationalized as follows. The microporous framework of $AlPO_4$-5 consists of strictly alternating AlO_4^- and PO_4^+ tetrahedra. The Al/P ratio of 1 creates an electronically neutral framework,[37] but the local electronegativity difference between Al and P induces a moderately polar interior. Although $AlPO_4$-5 molecular sieves are not regarded as acidic, several studies indicate a relatively weak but clearly present acidity of $AlPO_4$-5 frameworks.[38−40] The limited number of acid

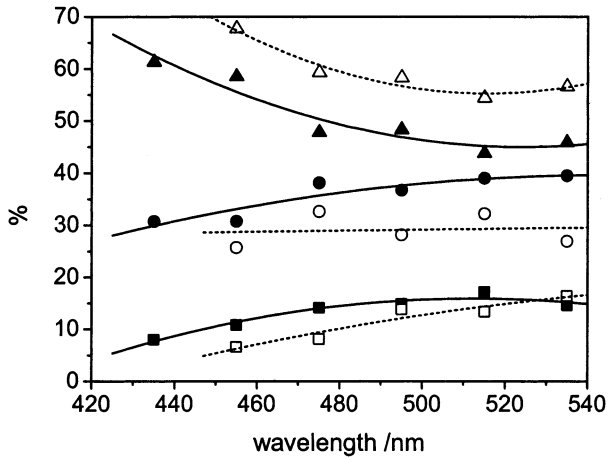

Figure 4. Emission wavelength-dependent contributions of the individual main peaks (fast components = squares, intermediate components = circles, slow components = triangles) within the decay time distributions of $BP(OH)_2$ in $AlPO_4$-5 (for a typical example, see Figure 3) excited at 393 (solid symbols) and 419 nm (open symbols). The lines are only guides to the eye and represent general trends.

sites is located on the surface of the crystals, as well as at defect sites.[41] There is evidence for both Brønsted and Lewis sites in $AlPO_4$-5, but the dominating acidity was attributed to terminal P−OH and Al−OH groups with weakly Brønsted acidic character.[42] Additionally, because of the hydrophilic character of the $AlPO_4$-5 framework, a large amount of water is coadsorbed into the channels of $AlPO_4$-5, which can influence the spectroscopic properties of incorporated guest molecules. In this respect, Ghanadzadeh and Zanjanchi proposed that guest−host interaction with the moderately polar framework should be of minor importance.[43]

$BP(OH)_2$ in Solution. For a better understanding of the data obtained in a confined medium, it is helpful to recollect the characteristic spectroscopic properties of $BP(OH)_2$ in liquid solution. In aprotic organic solvents, the excited-state features of $BP(OH)_2$ are dominated by a fast, concerted as well as stepwise,[44] excited-state intramolecular proton transfer (ESIPT), leading to a highly emissive zwitterionic double proton transfer state (Scheme 1) with a strongly Stokes-shifted fluorescence (ca. 10 000 cm^{-1}, Figure 5).[17] Because both the absorbing dienol and the emitting zwitterionic "pseudo-diketo" species have a very low dipole moment (cf. Scheme 1),[45] no solvatochromic tendencies can be observed. In protic solvents, however, the intramolecular hydrogen bonds have to compete with potentially H-bond-donating solvent molecules. As derived from the

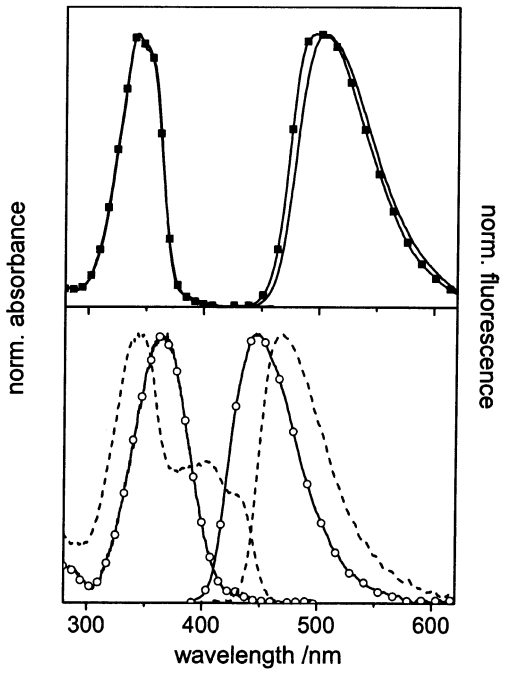

Figure 5. Steady-state spectra of $BP(OH)_2$ in the solvents *n*-hexane (—), dichloromethane (■) (upper part, absorption spectra are strongly overlapping), and neutral water (- — -), as well as the Zn^{II} complex of $BP(OH)_2$ in neutral water (○) (lower part) at 295 K.

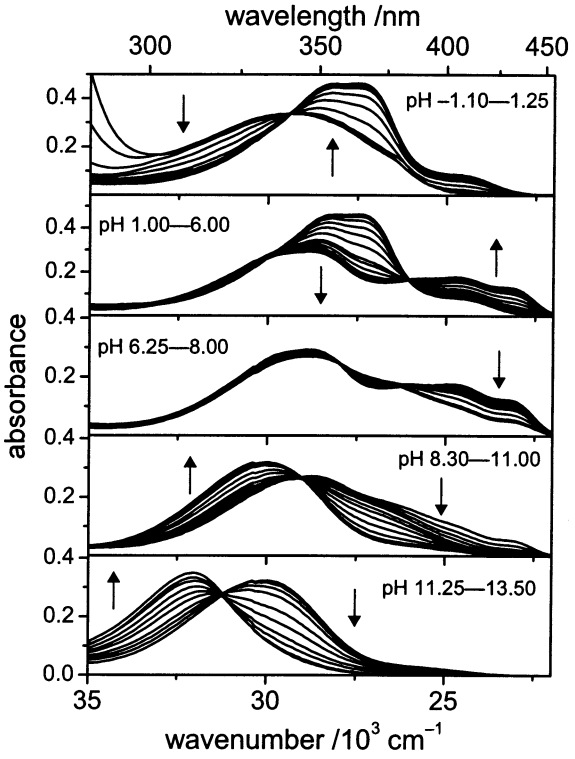

Figure 6. Spectrophotometric pH titration of $BP(OH)_2$ in water ($c_L = 1 \times 10^{-5}$ M; 50 mm quartz cells; arrows indicate directions of changes).

spectrophotometric data in Table 1, the ability of alcohols to form intermolecular hydrogen bonds already in the ground state is negligible (data in EtOH vs CH_2Cl_2). Upon excitation, ESIPT still occurs, but the reduced Stokes shift suggests that some interaction between the hydrogen-donating and -accepting centers of solvent and solute is encountered. Data of $BP(OH)_2$ in acetonitrile, with spectral features very similar to those in CH_2Cl_2 and $\Delta\tilde{\nu}_{abs-em} = 9700$ cm^{-1},[18c] and results reported by Marks et al., in which the mono-to-diketo conversion of $BP(OH)_2$ was found to be different in aprotic solvents (CH_2Cl_2, acetonitrile) as compared to ethanol,[46] support these assumptions. The changes are even more dramatic in water (Figure 5, Table 1). At neutral pH, the absorption spectrum is very broad and contains various subbands on the low-energy side. In contrast, the fluorescence spectrum consists of a major band reminiscent of the ESIPT band in organic solvents, but with a further reduced Stokes shift, and the fluorescence is still weaker as compared to ethanol. Time-resolved fluorescence measurements revealed biexponential decays in neutral water, but the second emitting and slower decaying species, which is found at the high-energy side of the spectrum, contributes to the total fluorescence with a relative amplitude of only ≤ 0.02. Thus, upon excitation at pH 6.4, most of the different Franck—Condon-excited conformers or tautomers undergo rapid transformation to the main emissive zwitterionic species (Figure 5). A theoretical treatment of the stabilization of the different forms of $BP(OH)_2$ by water molecules was recently published and these researchers put forward that in the ground state keto tautomers gain stability in the presence of water molecules with respect to the dienol form.[47]

Spectrophotometric Behavior as a Function of pH. Because hydrogen bonding and solvent proticity seem to play an important role in confined systems containing active hydroxyl groups, a spectrophotometric pH-titration study of the dye in solution should give some indication of the apparent nature of network—guest interaction. With the host being a hydrogen-bond donor rather than a hydrogen-bond acceptor, the acid-to-neutral pH region should allow us to derive the most important information. The UV/vis spectrophotometric pH titration spectra are shown in Figure 6. At very acidic pH, a single broad and structureless absorption band is found with a maximum at 340 nm (29 400 cm^{-1}). Upon increase of the pH to 1, the band's maximum shifts to 364 nm (27 500 cm^{-1}) and a shoulder appears at 403 nm (24 800 cm^{-1}). Whereas the absorption behavior is virtually unchanged between pH 1—2, the shape of the spectrum is drastically altered in the pH region of 2—4, with the global maximum found again at a shorter wavelength (347 nm; 28 800 cm^{-1}), a second maximum at 403 nm (24 800 cm^{-1}) and a shoulder at 431 nm (23 200 cm^{-1}). Throughout the medium pH range and up to pH $\approx$ 8, the situation remains unchanged, that is, complex absorption spectra composed of various subbands are noticed. The lower parts of Figure 6 suggests that only at pH > 9 a certain (deprotonated) tautomeric form strongly dominates, as indicated by the single-band absorption spectrum with a maximum at 333 nm (30 000 cm^{-1}). Increasing the basicity of the solution leads to build up of a band at 312 nm (32 000 cm^{-1}), most probably arising from doubly deprotonated $BP(O^-)_2$, and the appearance of an isosbestic point at 321 nm.

Analysis of the absorption spectra of $BP(OH)_2$ in water as a function of pH (Figure 6) applying principal component global analysis (PCGA) confirms the presence of three spectral components in the pH range from —1.1 to 6 with pK_a values of 0.16 and 2.69. At higher pH, two more pK_a's are found with values of 9.2 and 12.4. The pure spectra of the doubly protonated, monoprotonated, and neutral species as determined by PCGA are shown in Figure 7, together with experimental absorption profiles and their fits at three selected wavelengths including the corresponding residuals (Figure 8).

Fluorescence Behavior as a Function of pH. In acidic aqueous solution, $BP(OH)_2$ generally shows a moderate to high emission and at pH $\leq$ 2; excitation at any wavelength between 320 and 450 nm yields the same emission spectrum. A similar

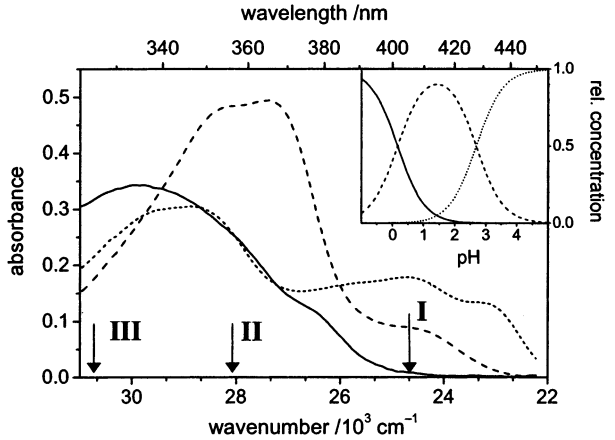

Figure 7. PCGA of the absorption pH titration spectra of $BP(OH)_2$ in water (cf. Figure 6) with a model function describing two acid−base equilibria with fitted pK_a values, pK_{a1} = 0.164 ± 0.004 and pK_{a2} = 2.688 ± 0.003, resolved spectra of the diprotonated (solid line), monoprotonated (dashed line), and neutral (dotted line) species. The insert shows the relative concentrations of the three species vs pH.

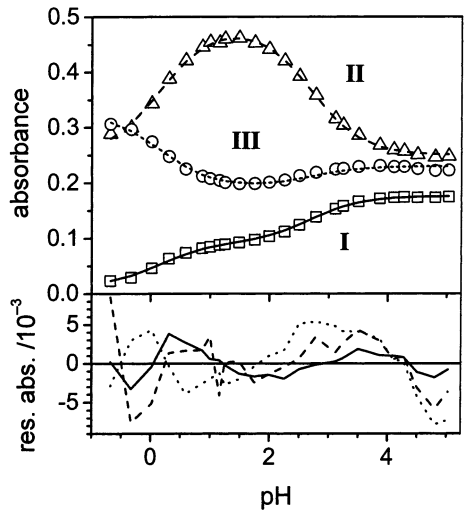

Figure 8. pH dependence (upper part) of the experimental (symbols) and the fitted (lines) absorbance at three spectral positions as indicated in Figure 7 (I = 25 000 cm^{-1}, II = 28 011 cm^{-1}, and III = 30 581 cm^{-1}) and (lower part) residual absorbance between the experimental and the fitted absorbance shown in the upper part (I = solid line, II = dashed line, III = dotted line).

behavior, that is, no wavelength dependences, is also observed for the fluorescence excitation spectra, thus always matching the absorption spectrum. This suggests that all of the different ground-state species undergo a fast (pseudo or real or both)[48] ESIPT reaction leading to the fluorescent diketo tautomer. In the pH region 2−4, the fluorescence quantum yield of $BP(OH)_2$ decreases steadily to reach a value of 0.04 at pH 4.

An analysis of the pH-dependent fluorescence lifetime of $BP(OH)_2$ as a function of excitation and emission wavelength yielded monoexponential decay behavior at pH < 3, consistent with steady-state spectroscopy. At pH > 3, the decays could only be fitted to (at least) two exponentials, but in neither case were rise times detected for any combination of excitation and emission wavelengths. Selected pH-dependent time-resolved emission data of $BP(OH)_2$ are summarized in Table S1.

Between pH 4 and 7, the steady-state emission spectra are only slightly blue-shifted as compared to the emission spectra in organic solvents and maintain their shape. The fluorescence quantum yield, $\Phi_f \approx 0.04$, is constant over a wide pH range. However, time-resolved fluorometry reveals a more complicated emission behavior. Here, a slow decay component with a (very) low relative amplitude, being dependent on excitation and emission wavelength, is detected throughout this pH range (Table S1). Because excitation at ca. 380 nm and detection at 440 nm yielded the largest relative amplitude for this component, the wavelength dependence of the slow decay component is obvious. The lack of rise times suggests that two or more species are simultaneously excited and two excited transient species emit in different regions of the spectrum.

Basicity changes the fluorescence properties of $BP(OH)_2$ even more strongly. The hypsochromically shifted shoulder at ca. 23 600 cm^{-1} already observed at medium pH gains in relative intensity, and its dependence on excitation wavelength is reflected by the fluorescence excitation spectra (Figure S4). Recording a fluorescence excitation spectrum with the emission monochromator set to the high-energy shoulder yields a spectrum centered at 27 500 cm^{-1}, whereas tuning the observation wavelength to 500 nm (20 000 cm^{-1}) reveals a fluorescence excitation spectrum resembling the absorption spectrum. These spectral changes are accompanied by a further decrease in fluorescence quantum yield and lifetime (Table 1, Table S1). At very basic pH, the fluorescence is almost completely quenched.

Spectroscopic Behavior in a Chemically Fixed State. A way to simulate a very tight intramolecular hydrogen bond and to study the spectroscopic properties of such a species, which is literally forced to perform proton transfer, is substitution of the hydroxyl proton by a diamagnetic metal ion that is able to form a stable six-membered N,O-chelate. Because we have recently carried out such investigations employing Zn^{II} and Cd^{II},[18c] the most important results for the present studies will be briefly described. When a (or both) hydrogen bond(s) is (are) replaced by a strongly coordinating unit such as a metal ion, the ground-state species diversity in aqueous solutions is again reduced, manifested by a single absorption band at ca. 365 nm (see spectrum of the Zn^{II} complex in Figure 5). The emission spectrum is also reminiscent of a single emitting species and appears at shorter wavelengths (Figure 5, Table 1). The fluorescence decay behavior of the Zn^{II} complex, which is strictly monoexponential also in water,[18c] suggests that replacement of the proton in the −O−H···N< fragment by a tightly binding chemical species protects the dye from hydrogen bond attack from the immediate environment. Moreover, the high fluorescence quantum yield of 0.62 indicates that a loss of fluorescence for the free dye molecule is most probably due to intramolecular motions.

Discussion

Liquid Media vs Zeolitic Host. In relation to $BP(OH)_2$ in aqueous surroundings, the spectroscopic features of zeolite-encapsulated $BP(OH)_2$ can be traced back to two main influences, the aqueous environment within $AlPO_4$-5 pores and guest−host interactions with a few relatively weak Brønsted acid sites of $AlPO_4$-5. The position of both the absorption and emission bands obtained by microscope-spectroscopic investigations of individual $BP(OH)_2$-containing $AlPO_4$-5 crystals and the resulting Stokes shift of 6300 cm^{-1} are virtually identical to those of the dye in an aqueous surrounding of pH ≈ 2 (Table 1, Figures 1 and 7; for a better comparison, the respective normalized spectra are combined in Figure S5). On the molecular scale, $BP(OH)_2$ with a size of 9.3 Å × 5 Å[49] occupies the $AlPO_4$-5 pores with a diameter of 7.3 Å.[14] Assuming that a water molecule requires ca. 1.5 Å,[49] the dye molecules do not

seem to be largely solvated in this particular zeolitic host, in contrast to, for instance, the microsolvation observed in sol−gel hosts with a pore size diameter of 26 Å.[50] For the latter host−guest ensemble, Prosposito et al. interpreted their time-resolved fluorescence results in such a way that, although a $BP(OH)_2$ molecule can only be surrounded by a few layers of solvent, in general, the solvent molecules still retain their motional freedom in the confined network and monoexponential decays are found on the nanosecond time scale. In the present case, the formation of an enveloping multilayer solvent shell is prevented by the much smaller dimensions of the intrazeolitic cavities, and by contrast, the single dye molecule might be even partly unsolvated and in immediate neighborhood of the host's inner surface. On the other hand, a comparison of the spectra obtained for the doped molecular sieves with those of $Zn^{II}\subset BP(OH)_2$ in solution suggests that, at least for the majority of the incorporated molecules, the bond between $BP(OH)_2$ and the host seems to be not as strong as that in a metal ion-bound complex (for a better comparison, see Figure S5).

However, besides the good agreement of the spectral band positions found for $BP(OH)_2$ in $AlPO_4$-5 and in acidic aqueous solution, the steady-state and especially the time-resolved emission data reveal some important differences, which do not allow us to classify the zeolite-incorporated species simply as monoprotonated dye molecules. The appearance of a hypsochromically shifted shoulder in emission obtained with laser excitation at 393 nm and the strong nonexponentiality of the fluorescence decay—note that the dye shows strictly monoexponential decays in water at pH ≤ 2—both favor an explanation of the observed features that involves more than one discrete chemical species. Again, the results obtained by Prosposito et al., that is, the above-mentioned monoexponential decays on the >10 ps time scale for $BP(OH)_2$ in sol−gel hosts with comparatively large pore sizes, support the present results. The highly constrained pore structure of $AlPO_4$-5 forces the dye molecules to interact with coadsorbed water or the wall, creating an apparent acidity. As in the case of $BP(OH)_2$ in aqueous solution at pH > 4, the slowly decaying component (with $\tau_f \approx$ 3.6 ns in the present case) is responsible for the shoulder at the high-energy side of the fluorescence spectrum (Figure 4) and, by analogy, should not originate from protonation. Moreover, the absence of rise times on the >10 ps time range indicates that this minor component does not convert into one of the other two emissive forms during the lifetime of the excited state, both in $AlPO_4$-5 and in water at pH > 4. Apparently, the same fact implies that also the other two species found for $BP(OH)_2$ in $AlPO_4$-5 are not products of an excited-state photochemical reaction on this time scale. The three decay components can thus be attributed to the presence of (at least) three spectrally largely overlapping ground-state species, the slight differences in ground-state population being directly evident from the amplitude changes between the 393 and 419 nm excitation data (solid and open symbols in Figure 4).

More information on the species diversity involved can be obtained by a closer inspection of the results of the fluorescence lifetime data analyses, involving measured and simulated data.[51] In the present case, we tested eight different pairs of real and simulated decays and found that the lifetime distribution model is especially suited to describe the emitting species centered around the two maxima at shorter average lifetimes.[51] Only a minority of the $BP(OH)_2$ molecules seems to be located in a rather strongly interacting environment and shows a comparatively slow fluorescence decay with an excitation and emission wavelength dependence more similar to a chemically fixed or metal ion-bound species and the minor component of free $BP(OH)_2$ in aqueous solution. Although the exact chemical nature of this species is still unclear, recent investigations on the photophysics of the monohydroxy derivative 2,2′-bipyridyl-3-ol in water as a function of pH suggest that certain zwitterionic species, probably stabilized by water molecules, might be responsible for this long-lived emission.[52] However, for the majority of the dye molecules, which show a fast emissive decay to the ground state more reminiscent of $BP(OH)_2$ in aqueous acidic-to-neutral solution, the results presented suggest that the strong intramolecular hydrogen bonds usually observed in aprotic solvents are (partially) disrupted and the stabilization is thus reduced. On the basis of the similarity of the spectral features and the fluorescence lifetimes of 0.7−0.8 ns of the intermediate average lifetime component and the free molecule at acidic pH, this emission is attributed to species strongly interacting with coadsorbed water molecules, as well as with Brønsted acidic sites of the host's wall. Finally, it remains to be investigated with femtosecond spectroscopic methods to what instance the presence of different ground-state keto or enol tautomers or both can account for the observed three maxima in the lifetime distribution function.

Conclusion

In the present article, we have shown that $AlPO_4$-5 molecular sieves doped with 2,2′-bipyridyl-3,3′-diol present a stable fluorescent composite material with a high degree of alignment of the guest molecules within the host's pore system, resulting in a pronounced optical anisotropy. These features along with a comparatively strong fluorescence,[53] as well as similar spectra of single crystals and crystal ensembles and a promising but yet not systematically investigated photostability, suggest that these materials may be suited as spectral fluorescence standards[54] for microfluorometric applications.[55,56] In the present case, a comparison of the spectroscopic properties of the solid-state material with those of the dye in solution also allowed us to derive some general insights on the interaction of host and incorporated guest. Although the fluorescence decay behavior of the doped crystals is strongly heterogeneous, the two main influences, the presence of coadsorbed water molecules and a few weakly Brønsted acidic defect sites, do not have a pronounced effect on the envelope of the emission spectrum. Apparently, this is advantageous in terms of simplicity and handling of such composite materials in fluorescence-based applications.

Acknowledgment. We thank Dr. F. Marlow, MPI für Kohlenforschung Mülheim/Ruhr for stimulating discussions. Cooperation and support by Prof. H. Baumgärtel (Free University Berlin) and the ACA Berlin-Adlershof are gratefully acknowledged. The authors thank Prof. W. Rettig for use of the time-resolved fluorescence setup at BESSY, I. Girnus for molecular sieve crystals, E. Biller for technical assistance, and the Deutsche Forschungsgemeinschaft for financial support.

Supporting Information Available: Graphical determination of pK_a, sample chamber setup, and various additional spectral and lifetime data including six figures and one table. This material is available free of charge via the Internet at http://pubs.acs.org.

References and Notes

(1) Wolarz, E.; Kilian, D.; Haase, W.; Bauman, D. *J. Polym. Sci., Part B: Polym. Phys.* **1999**, *37*, 369. Müller, M.; Zentel, R.; Maka, T.; Romanov, S. G.; Sotomayor Torres, C. M. *Chem. Mater.* **2000**, *12*, 2508.

(2) Scaiano, J. C.; García, H. *Acc. Chem. Res.* **1999**, *32*, 783. Reisfeld, R. *Opt. Mater.* **2001**, *16*, 1.

(3) Hou, Z. J.; Liu, L. Y.; Xu, L.; Xu, Z. L.; Wang, W. C.; Li, F. M.; Ye, M. X. *Chem. Mater.* **1999**, *11*, 3177. Maggini, M.; De Faveri, C.; Scorrano, G.; Prato, M.; Brusatin, G.; Guglielmi, M.; Meneghetti, M.; Signorini, R.; Bozio, R. *Chem.—Eur. J.* **1999**, *5*, 2501.

(4) Charlton, A.; McKinnie, I. T.; Menesses-Nava, M. A.; King, T. A. *J. Mod. Opt.* **1992**, *39*, 1517. Lebeau, B.; Herlet, N.; Livage, J.; Sanchez, C. *Chem. Phys. Lett.* **1993**, *206*, 15. Przhonska, O. V. In *Near-Infrared Dyes for High Technology Applications;* Daehne, S., Resch-Genger, U., Wolfbeis, O. S., Eds.; Kluwer Academic: Dordrecht, Netherlands, 1998; pp 265−285. Vietze, U.; Krauss, O.; Laeri, F.; Ihlein, G.; Schüth, F.; Limburg, B.; Abraham, M. *Phys. Rev. Lett.* **1998**, *81*, 4628. Peng, G.-D.; Li, A. D. Q. *J. Polym. Sci., Part B: Polym. Phys.* **2001**, *39*, 1794.

(5) Feringa, B. L.; Jager, W. F.; de Lange, B. *Tetrahedron* **1993**, *49*, 8267. Wang, G.; Hou, L.; Gan, F. *Phys. Status Solidi A* **1999**, *174*, 269.

(6) Mager, L.; Melzer, C.; Barzoukas, M.; Fort, A.; Mery, S.; Nicoud, J.-F. *Appl. Phys. Lett.* **1997**, *71*, 2248. Hoffmann, K.; Marlow, F.; Caro, J. *Adv. Mater.* **1997**, *9*, 567. Hoffmann, K.; Resch-Genger, U.; Marlow, F. *Microporous Mesoporous Mater.* **2000**, *41*, 99.

(7) Pauchard, M.; Devaux, A.; Calzaferri, G. *Chem.—Eur. J.* **2000**, *6*, 3456.

(8) Ganesan, V.; John, S. A.; Ramaraj, R. *J. Electroanal. Chem.* **2001**, *502*, 167.

(9) For zeolite-based systems, see, for example: Meinershagen, J. L.; Bein, T. *J. Am. Chem. Soc.* **1999**, *121*, 448. For sol−gel-based systems, see, for example: Chernyak, V.; Reisfeld, R.; Gvishi, R.; Venezky, D. *Sens. Mater.* **1990**, *2*, 117. MacCraith, B. D.; Ruddy, V.; Potter, C.; O'Kelly, B.; McGilp, J. F. *Electron. Lett.* **1991**, *27*, 1247. For polymer-based systems see, for example: Mohr, G. J.; Nezel, T.; Spichiger-Keller, U. E. *Anal. Chim. Acta* **2000**, *414*, 181. Lu, X.; Manners, I.; Winnik, M. A. In *New Trends in Fluorescence Spectroscopy: Applications to Chemical and Life Sciences*; Valeur, B., Brochon, J.-C., Eds.; Springer: Berlin, 2001; pp 229−255.

(10) Calzaferri, G.; Gfeller, N. *J. Phys. Chem.* **1992**, *96*, 3428.

(11) Ganschow, M.; Wark, M.; Wöhrle, D.; Schulz-Ekloff, G. *Angew. Chem., Int. Ed.* **2000**, *39*, 160.

(12) Schulz-Ekloff, G. *Stud. Surf. Sci. Catal.* **1994**, *85*, 145. Gabelica, Z.; Valange, S.; Shibata, M.; Hotta, H.; Suzuki, T. *Microporous Mesoporous Mater.* **2001**, *44*−*45*, 645.

(13) Scaiano, J. C.; Kaila, M.; Corrent, S. *J. Phys. Chem. B* **1997**, *101*, 8564. Uppili, S.; Thomas, K. J.; Crompton, E. M.; Ramamurthy, V. *Langmuir* **2000**, *16*, 265. Marquez, F.; Zicovich-Wilson, C. M.; Palomares, E.; Garcia, H. *J. Phys. Chem. B* **2001**, *105*, 9973. Kalyanasundaram, K. In *Photochemistry in Organized and Constrained Media*; Ramamurthy, V., Ed.; VCH: New York, 1991; pp 39−79. Pauchard, M.; Huber, S.; Mealllet-Renault, R.; Maas, H.; Pansu, R.; Calzaferri, G. *Angew. Chem., Int. Ed.* **2001**, *40*, 2839.

(14) $AlPO_4$-5 (AFI type; Meier, W. M.; Olson, D. H.; Baerlocher, C. *Atlas of Zeolite Structure Types*, 4th rev. ed.; Butterworth-Heinemann: New York, 1996; pp 26 and 146.) possesses a hexagonal symmetry and a one-dimensional channel system with a 12-membered circular pore of 7.3 Å free opening running parallel to the crystal's hexagonal axis.

(15) Sepiol, J.; Bulska, H.; Grabowska, A. *Chem. Phys. Lett.* **1987**, *140*, 607. Kaczmarek, L.; Nowak, B.; Zukowski, J.; Borowicz, P.; Sepiol, J.; Grabowska, A. *J. Mol. Struct.* **1991**, *248*, 189.

(16) Bulska, H. *J. Lumin.* **1988**, *39*, 293.

(17) Bulska, H.; Grabowska, A.; Grabowski, Z. R. *J. Lumin.* **1986**, *35*, 189.

(18) (a) Johansson, L. B.-Å.; Persson, L.; Langhals, H. *J. Chem. Soc., Faraday Trans.* **1996**, *92*, 4909. (b) Vollmer, F.; Rettig, W. *J. Photochem. Photobiol. A* **1996**, *95*, 143. (c) Rurack, K.; Radeglia, R. *Eur. J. Inorg. Chem.* **2000**, 2271.

(19) Girnus, I.; Jancke, K.; Vetter, R.; Richter-Mendau, J.; Caro, J. *Zeolites* **1995**, *13*, 33.

(20) Resch, U.; Rurack, K. *Proc. SPIE-Int. Soc. Opt. Eng.* **1997**, *3105*, 96.

(21) Rurack, K.; Bricks, J. L.; Schulz, B.; Maus, M.; Reck, G.; Resch-Genger, U. *J. Phys. Chem. A* **2000**, *104*, 6171.

(22) Vogel, M.; Rettig, W. *Ber. Bunsen-Ges. Phys. Chem.* **1987**, *91*, 1241.

(23) Al-Soufi, W.; Novo, M.; Mosquera, M. *Appl. Spectrosc.* **2001**, *55*, 630.

(24) It is important to note that the spectra obtained for individual crystals and for crystal ensembles or powder samples were identical.

(25) Bulska, H. *Chem. Phys. Lett.* **1983**, *98*, 398.

(26) Hoffmann, K.; Marlow, F.; Caro, J. *Zeolites* **1996**, *16*, 281.

(27) The samples were exposed to pulsed laser light of 60 mJ pulse peak power (4 MHz repetition rate) for 60 min.

(28) Löfroth, J.-E. *J. Phys. Chem.* **1986**, *90*, 1160. Rurack, K.; Resch-Genger, U.; Rettig, W. *J. Photochem. Photobiol. A* **1998**, *118*, 143.

(29) Eight (for a single excitation series) or 16 decays (for a combined analysis of data excited at 393 and 419 nm) were globally analyzed. In the latter case, with a simultaneous analysis of all of the decays measured, lifetimes of 0.12, 0.69, and 3.45 ns gave the best results (global $\chi_R^2 = 1.15$).

(30) Kollmannsberger, M.; Rurack, K.; Resch-Genger, U.; Daub, J. *J. Phys. Chem. A* **1998**, *102*, 10211.

(31) Quasi-continuous refers to the finite number of single lifetimes that the software employed allows to fit to a given set of data. In our case, with the FLA900 program package allowing us to include between 20 and 100 lifetimes, we obtained the best results with the maximum number of lifetimes.

(32) Ware, W. R. In *Photochemistry in Organized and Constrained Media*; Ramamurthy, V., Ed.; VCH: New York, 1991; pp 563−602.

(33) Bright, F. V.; Catena, G. C.; Huang, J. *J. Am. Chem. Soc.* **1990**, *112*, 1343.

(34) James, D. R.; Liu, Y.-S.; De Mayo, P.; Ware, W. R. *Chem. Phys. Lett.* **1985**, *120*, 460.

(35) Fritz, R.; Kungl, A.; Rettig, W.; Springer, J. *Chem. Phys. Lett.* **1996**, *260*, 409. Spitz, C.; Dähne, S. *Ber. Bunsen-Ges. Phys. Chem.* **1998**, *102*, 738.

(36) It is interesting to note that comparable trends are found upon analysis of the emission wavelength dependence of the relative quantum yields of the discrete species obtained by global fitting routines.

(37) Bennett, J. M.; Dytrych, W. J.; Pluth, J. J.; Richardson, J. W.; Smith, J. V. *Zeolites* **1996**, *6*, 349.

(38) Akolekar, D. B. *Zeolites* **1994**, *14*, 53.

(39) Akolekar, D. B.; Huang, M.; Kaliaguine, S. *Zeolites* **1994**, *14*, 519.

(40) Lei, Z.; Vaidyalingam, A.; Dutta, P. K. *J. Phys. Chem. B* **1998**, *102*, 8557.

(41) Hedge, S. G.; Ratnasamy, P.; Kustov, L. M.; Kazansky, V. B. *Zeolites* **1988**, *8*, 137.

(42) Müller, G. *J. Mol. Struct.* **1997**, *410*−*411*, 173.

(43) Ghanadzadeh, A.; Zanjanchi, M. A. *Spectrochim. Acta, Part A* **2001**, *57*, 1865.

(44) Zhang, H.; van der Meulen, P.; Glasbeek, M. *Chem. Phys. Lett.* **1996**, *253*, 97. Marks, D.; Prosposito, P.; Zhang, H.; Glasbeek, M. *Chem. Phys. Lett.* **1998**, *289*, 535. Neuwahl, F. V. R.; Foggi, P.; Brown, R. G. *Chem. Phys. Lett.* **2000**, *319*, 157.

(45) Borowicz, P.; Grabowska, A.; Wortmann, R.; Liptay, W. *J. Lumin.* **1992**, *52*, 265.

(46) Marks, D.; Zhang, H.; Glasbeek, M.; Borowicz, P.; Grabowska, A. *Chem. Phys. Lett.* **1997**, *275*, 370.

(47) Carballeira, L.; Perez-Juste, I. *J. Mol. Struct. (THEOCHEM)* **1996**, *368*, 17.

(48) "Pseudo" here implies that in protonated species, when the hydroxyl oxygen atom becomes more acidic in S_1 (Waluk, J.; Bulska, H.; Grabowska, A.; Mordzinski, A. *New J. Chem.* **1986**, *10*, 413.), upon excitation, a simple deprotonation step can lead to the formation of the emissive zwitterionic tautomer. This was experimentally confirmed by a comparative study of $BP(OH)_2$ and the corresponding "ground-state diketo tautomer", 1,1′-dimethyl-3,3′-dioxido-[2,2′-bipyridinium] (DDB), yielding a very different ground-state but a very similar excited-state behavior (Borowicz, P.; Grabowska, A.; Kaczmarek, L.; Lés, A.; Adamowicz, L. *Chem. Phys. Lett.* **1995**, *239*, 282.). Furthermore, the band positions of 28 500 cm^{-1} (abs) and 20 700 cm^{-1} (em) of DDB closely resemble those found by us for $BP(OH)_2$ in the pH 2 region and the fluorescence quantum yields (0.032 for DDB vs ∼0.06 for $BP(OH)_2$ at pH ≈ 2) and lifetimes (0.74 ns for DDB and ∼0.7 ns for $BP(OH)_2$ at pH ≈ 2) are also very similar.

(49) On the basis of the AM1-optimized ground-state geometry (AMPAC V6.55, Semichem, Inc.).

(50) Prosposito, P.; Marks, D.; Zhang, H.; Glasbeek, M. *J. Phys. Chem. A* **1998**, *102*, 8894.

(51) A possibility to test whether the application of a lifetime distribution function is justified to model the fluorescence deactivation of $BP(OH)_2$ incorporated in $AlPO_4$-5 is the comparison of real and simulated decays (Wang, H.; Harris, J. M. *J. Phys. Chem.* **1995**, *99*, 16999.). Here, for a certain pair of instrumental response function (IRF) and measured fluorescence decay (MFD), the results of a triple exponential fit of the actual decay are convoluted with the IRF to give the simulated decay (including the addition of sufficient artifical noise when creating the synthetic decay). The latter is then analyzed employing a lifetime distribution fitting routine. When the fit of this procedure is virtually similar to a distribution analysis obtained for the original IRF/MFD combination, the system can be described sufficiently by a discrete decay model. If both distributions functions are substantially different, the impact of the microenvironment on the photophysics of the system is not negligible and permits us to invoke a model based on species heterogeneity. In the present case, we tested eight different pairs of real and simulated decays and for every comparison obtained a significantly smaller species distribution for the simulated decay than for the MFD, exemplified by an average $\langle\tau\rangle/\sigma$ ratio of >5 for the simulated as

compared to ~2.5 for the measured decay (for a graphic example, see Figure S6). The deviation was found to be especially pronounced for the two maxima at shorter average lifetimes.

(52) Rurack, K.; Al-Soufi, W. *Book of Abstracts XVIII IUPAC Symposium on Photochemistry*; Technische Universität Dresden: Dresden, Germany, 2000; pp 523−524 (full manuscript currently in preparation).

(53) Via analogy of the mean fluorescence lifetimes and with the assumption that the radiative rate constants of the species in liquid and confined media are largely similar, Φ_f is estimated to ~0.08.

(54) Velapoldi, R. A.; Mielenz, K. D. *NBS Spec. Publ.* **1980**, *260*−*264*. Gardecki, J. A.; Maroncelli, M. *Appl. Spectrosc.* **1998**, *52*, 1179.

(55) Velapoldi, R. A.; Epstein, M. S. In *Luminescence Applications in Biological, Chemical, Environmental, and Hydrological Sciences*; Goldberg, M. C., Ed.; ACS Symposium Series 383, American Chemical Society: Washington, DC, 1989; pp 98−126.

(56) Ploem, J. S. In *Fluorescent and Luminescent Probes for Biological Activity*, 2nd ed.; Mason, W. T., Ed.; Academic: San Diego, CA, 1999; pp 3−13. Haupts, U.; Rüdiger, M., Pope, A. J. *Drug Discovery Today* **2000**, *1* (HTS Suppl.), 3. Hessling, M.; Ihlemann, J.; Marowsky, G. *Rev. Sci. Instrum.* **2000**, *71*, 2201.